PHYSICS

Search for exotic spin-dependent interactions with a spin-based amplifier

Haowen Su[1,2,3]†, Yuanhong Wang[1,2,3]†, Min Jiang[1,2,3]*, Wei Ji[4], Pavel Fadeev[5,6], Dongdong Hu[7], Xinhua Peng[1,2,3]*, Dmitry Budker[5,6,8]

Copyright © 2021 The Authors, some rights reserved; exclusive licensee American Association for the Advancement of Science. No claim to original U.S. Government Works. Distributed under a Creative Commons Attribution NonCommercial License 4.0 (CC BY-NC).

Development of new techniques to search for particles beyond the standard model is crucial for understanding the ultraviolet completion of particle physics. Several hypothetical particles are predicted to mediate exotic spin-dependent interactions between standard-model particles that may be accessible to laboratory experiments. However, laboratory searches are mostly conducted for static spin-dependent interactions, with a few experiments addressing spin- and velocity-dependent interactions. Here, we demonstrate a search for these interactions with a spin-based amplifier. Our technique uses hyperpolarized nuclear spins as an amplifier for pseudo-magnetic fields produced by exotic interactions by a factor of more than 100. Using this technique, we establish constraints on the spin- and velocity-dependent interactions between polarized neutrons and unpolarized nucleons for the force range of 0.03 to 100 meters, improving previous constraints by at least two orders of magnitude in partial force range. This technique can be further extended to investigate other exotic spin-dependent interactions.

INTRODUCTION

Numerous theories extending beyond the standard model of particle physics predict the existence of new bosons that could mediate long-range interactions between two objects of the standard model (*1*–*5*). Such theories are related with the spontaneous breaking of continuous symmetries, yielding massless or light (pseudo) Nambu-Goldstone bosons, such as axions (*2*, *3*), dark photons (*6*), paraphotons (*7*), familons (*8*), and majorons (*9*). The exchange of such particles results in exotic spin-dependent interactions that may be accessible to laboratory experiments (*10*, *11*). Various experiments have been conducted to search for exotic spin-dependent interactions, making use of the torsion balance (*12*, *13*), trapped ions (*14*, *15*), geoelectrons (*16*, *17*), spin-exchange relaxation-free magnetometers (*18*, *19*), comagnetometers (*20*, *21*), nitrogen-vacancy diamond (*22*–*24*), and other high-sensitivity techniques (*25*–*32*). Recently, the approach based on nuclear magnetic resonance (NMR) (*33*–*35*) has been proposed to search for exotic interactions and could substantially improve current experimental limits set by astrophysics, such as axion resonant interaction detection experiment (ARIADNE) (*35*).

The exotic interactions mediated by light bosons were introduced by Moody and Wilczek (*36*), extended by Dobrescu and Mocioiu (*37*) with the inclusion of the terms dependent on the relative velocity between the two interacting particles, and revised in (*5*). In the latter work (*5*), the potentials were sorted by types of coupling (scalar, vector, etc.), contact interactions were included, and coordinate-space representation was used. Sorting by spin-momentum form, there are 15 possible exotic interactions between ordinary particles that contain static spin-dependent operators, velocity-dependent operators, or combinations of these. Some of them may break the charge, parity, and time-reversal symmetries or their combinations (*11*, *37*); they were introduced to understand the symmetries of charge conjugation and parity in quantum chromodynamics (*3*). Many experiments have been performed to search for static spin-dependent interactions (*12*, *14*–*16*, *20*–*23*, *25*, *26*, *29*, *31*, *32*), while the velocity-dependent interactions have been studied less extensively (*18*, *19*, *24*, *28*, *30*). Following the notation in (*37*, *38*), the spin- and velocity-dependent interactions to be studied here are

$$V_{4+5} = -f_{4+5}\frac{\hbar^2}{8\pi mc}[\hat{\sigma}\cdot(\boldsymbol{v}\times\hat{r})]\left(\frac{1}{\lambda r}+\frac{1}{r^2}\right)e^{-r/\lambda} \quad (1)$$

$$V_{12+13} = f_{12+13}\frac{\hbar}{8\pi}(\hat{\sigma}\cdot\boldsymbol{v})\left(\frac{1}{r}\right)e^{-r/\lambda} \quad (2)$$

where f_{4+5} and f_{12+13} are dimensionless coupling constant, c is the speed of light in vacuum, $\hat{\sigma}$ is the spin vector and m is the mass of the polarized fermion, $\boldsymbol{v}$ is the relative velocity between two interacting fermions, $\hat{r}$ is the unit vector in the direction between them, and $\lambda = \hbar(m_b c)^{-1}$ is the force range (or the boson Compton wavelength) with m_b being the light boson mass. In particular, apart from common interests on the interaction V_{4+5} mediated by new bosons described in (*37*), the search for V_{4+5} could provide an experimental test for extensions of electrodynamics proposed by a recent study (*39*). Moreover, the search for V_{12+13} could provide a new source for parity symmetry violation (*11*, *37*). Careful investigations on those interactions may give clues for understanding fundamental physical questions such as the matter-antimatter asymmetry of the universe.

Here, we demonstrate a search for the exotic spin- and velocity-dependent interactions with a spin-based amplifier (*40*). The technique takes advantage of the resonant coupling between the rotation frequency of an unpolarized nucleon mass and a spin-based amplifier with a matching spin-precession frequency. The signal from the pseudo-magnetic field produced by the exchange of light bosons can be amplified by at least two orders of magnitude. Using such a spin-based amplifier, we establish constraints on the spin- and

[1]Hefei National Laboratory for Physical Sciences at the Microscale and Department of Modern Physics, University of Science and Technology of China, Hefei, Anhui 230026, China. [2]CAS Key Laboratory of Microscale Magnetic Resonance, University of Science and Technology of China, Hefei, Anhui 230026, China. [3]Synergetic Innovation Center of Quantum Information and Quantum Physics, University of Science and Technology of China, Hefei, Anhui 230026, China. [4]Department of Physics, Tsinghua University, Beijing, 100084, China. [5]Helmholtz-Institut, GSI Helmholtzzentrum für Schwerionenforschung, Mainz 55128, Germany. [6]Johannes Gutenberg University, Mainz 55128, Germany. [7]State Key Laboratory of Particle Detection and Electronics, University of Science and Technology of China, Hefei, Anhui 230026, China. [8]Department of Physics, University of California, Berkeley, Berkeley, CA 94720-7300, USA.
*Corresponding author. Email: dxjm@ustc.edu.cn (M.J.); xhpeng@ustc.edu.cn (X.P.)
†These authors contributed equally to this work.

Downloaded from https://www.science.org at Helmholtzzentrum fuer Schwerionenforschung GmbH on January 10, 2022

velocity-dependent interactions between polarized and unpolarized nucleons in the force range of 0.03 to 100 m. For f_{4+5}, our work sets the most stringent constraints on f_{4+5} for the force range from 0.04 to 100 m. For λ=1.0 m, our work improves over existing constraints by about four orders of magnitude (*41*, *42*). Moreover, our work sets the most stringent constraints on f_{12+13} in the force range from 0.05 to 6 m, at 0.45 m reaching 1.01×10^{-34} [95% confidence level (C.L.)], improving over previous laboratory limits by at least two orders of magnitude (*43*, *44*).

We would like to emphasize the difference of resonant searches between this work and other existing works. Although, recently, there have been many works that propose the NMR resonant searches of the exotic spin-dependent interactions (*33*–*35*), their experimental demonstrations are ongoing. In contrast, our work demonstrates an experiment of the resonance detection method to search for exotic spin-dependent interactions and places new constraints on them. Moreover, previous works all consider the situation where the nuclear spins are measured from a distance with atomic and superconducting quantum interference device magnetometers; in this case, it is experimentally challenging to prepare high nuclear-spin polarization and maintain readout sensitivity. In contrast, our work uses a different scheme in which polarized nucleons and the detector are spatially overlapping in the same vapor cell, offering two notable advantages (see section SIV): Nuclear spins can be directly hyperpolarized to achieve a polarization of 0.1 to 0.3 by spin-exchange optical pumping, reducing the polarization loss during transporting nuclear spins to detection region; nuclear spin signals can be enhanced due to large Fermi-contact enhancement (on the order of 600), measured in situ with an atomic magnetometer. Using such a sensor, we immediately obtain new constraints on the spin- and velocity-dependent interactions.

RESULTS

Principle

Our experiment is to detect the pseudo-magnetic field produced by exotic spin- and velocity-dependent interactions. These interactions induce energy shift of ^{129}Xe spins $-\boldsymbol{\mu}_{\mathrm{Xe}} \cdot \mathbf{B}_j^{\mathrm{exo}} = V_j$ (*29*), where $\boldsymbol{\mu}_{\mathrm{Xe}}$ is the magnetic moment of ^{129}Xe spin, V_j represents the potential that we measure (V_{4+5} or V_{12+13}), and $\mathbf{B}_j^{\mathrm{exo}}$ is the pseudo-magnetic field. As is typical (*18*, *21*), we assume that the coupling to unpolarized fermions is the same for neutrons and protons and is 0 for electrons in the unpolarized mass. We note that the contribution of neutrons is 73% in ^{129}Xe (*45*) and therefore set $|\boldsymbol{\mu}_{\mathrm{Xe}}||\mathbf{B}_j^{\mathrm{exo}}| > f_j 0.73A$, where A is the numerical factor from the integration over all the nucleons in the bismuth germanate insulator $Bi_4Ge_3O_{12}$ (BGO) crystal (see Materials and Methods), and f_j represents f_{4+5} and f_{12+13}.

The pseudo-magnetic field is resonantly measured with the spin-based amplifier consisting of the spatially overlapping ensembles of spin-polarized ^{87}Rb and ^{129}Xe, as shown in Fig. 1. ^{129}Xe spins act as an amplifier for the signal from the oscillating pseudo-magnetic field. The field $\mathbf{B}_j^{\mathrm{exo}}$ slightly tilts ^{129}Xe spins and induces an oscillating ^{129}Xe transverse magnetization that is read out by ^{87}Rb spins. The spin dynamics can be described by the coupled Bloch equations (*19*, *40*, *46*)

$$\frac{\partial \mathbf{P}^e}{\partial t} = \frac{\gamma_e}{Q}(B_z^0\hat{z} + \beta M_0^n \mathbf{P}^n) \times \mathbf{P}^e + \frac{P_0^e\hat{z} - \mathbf{P}^e}{T_e Q} \quad (3)$$

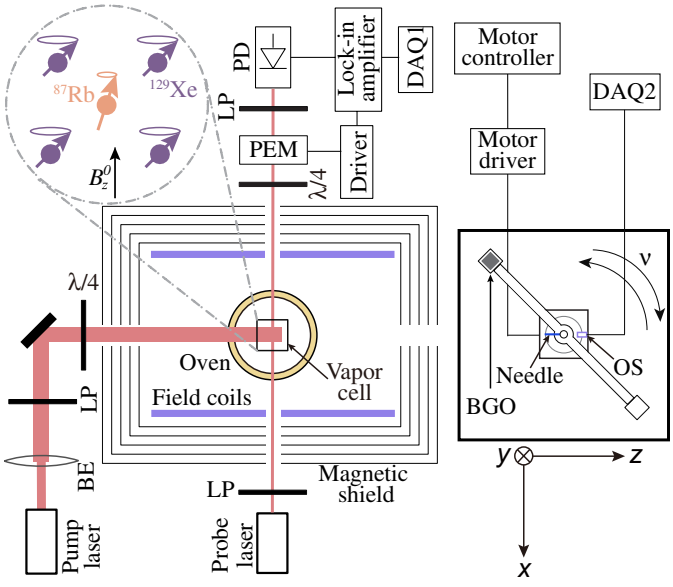

Fig. 1. Experimental setup. The ^{87}Rb magnetometer uses a 0.5-cm^3 cubic cell consisting of 5 torr isotopically enriched ^{129}Xe, 250 torr N_2 as buffer gas, and a droplet of ^{87}Rb. The vapor cell is placed inside a five-layer cylindrical μ-metal shield to reduce the ambient magnetic field. A bias field $B_z^0\hat{z}$ is applied along z to tune the ^{129}Xe Larmor frequency to $\nu_0 \approx 4.995$ Hz. The ^{87}Rb spins are polarized by optical pumping with 795-nm D1 light. ^{87}Rb-^{129}Xe spin-exchange collisions polarize ^{129}Xe spins to ~30% (*40*, *47*). The x component of ^{87}Rb spins is measured via optical rotation of a linearly polarized probe beam (*54*–*57*), which is blue-detuned 110 GHz to ^{87}Rb D2 transition at 780 nm. The right inset shows the configuration of a bismuth germanate insulator [$Bi_4Ge_3O_{12}$ (BGO)] mass and a motor. A single BGO mass at the end of an aluminum rod rotates with frequency $\nu_0 \approx 4.995$ Hz to generate the spin- and velocity-dependent interactions. BE, beam expander; LP, linear polarizer; λ/4, quarter–wave plate; PD, photodiode; PEM, photoelastic modulator; DAQ, data acquisition; OS, optoelectronic switch.

$$\frac{\partial \mathbf{P}^n}{\partial t} = \gamma_n(B_z^0\hat{z} + \mathbf{B}_j^{\mathrm{exo}} + \beta M_0^e \mathbf{P}^e) \times \mathbf{P}^n + \frac{P_0^n\hat{z} - \mathbf{P}^n}{\{T_{2n}, T_{2n}, T_{1n}\}} \quad (4)$$

where $\mathbf{P}^e$ ($\mathbf{P}^n$) is the polarization of ^{87}Rb electron (^{129}Xe nucleus), γ_e (γ_n) is the gyromagnetic radio of the ^{87}Rb electron (^{129}Xe nucleus), Q is the electron slowing-down factor that originated from hyperfine interaction and spin-exchange collisions, $B_z^0\hat{z}$ is the applied bias field; M_0^e (M_0^n) is the maximum magnetization of ^{87}Rb electron (^{129}Xe nucleus) associated with full spin polarizations, P_0^e (P_0^n) is the equilibrium polarization of the ^{87}Rb electron (^{129}Xe nucleus), T_e is the common relaxation time of ^{87}Rb electron spins, and T_{1n} (T_{2n}) is the longitudinal (transverse) relaxation time of ^{129}Xe spins. The Fermi-contact interaction between ^{87}Rb and ^{129}Xe pairs introduces an effective magnetic field $\mathbf{B}_{\mathrm{eff}}^{e,n} = \beta M_0^{e,n} \mathbf{P}^{e,n}$, where $\beta = 8\pi\kappa_0/3$ (*40*, *46*, *47*). The effective field generated by ^{129}Xe spins is read out in situ with the ^{87}Rb magnetometer.

We first consider the resonant response of the spin-based amplifier to a single-frequency component, for example, $\mathbf{B}_{\mathrm{ac}}^{\mathrm{exo}} = B_{\mathrm{ac}}^{\mathrm{exo}} \cos(2\pi\nu t)\,\hat{y}$ of the pseudo-magnetic field $\mathbf{B}_j^{\mathrm{exo}}$. In this situation, the bias field $B_z^0\hat{z}$ is tuned to satisfy the resonant condition $\nu = \nu_0 = \gamma_n B_z^0/(2\pi)$. Because of negligible $\mathbf{B}_{\mathrm{eff}}^e$ and relatively strong bias field $B_z^0\hat{z}$, ^{129}Xe spins independently evolve without the influence of ^{87}Rb spins. For small transverse excitations of ^{129}Xe spins, we can derive the steady-state solution of ^{129}Xe transverse polarization from Eq. 4. A detailed derivation can be found in the Supplementary Materials (section

Downloaded from https://www.science.org at Helmholtzzentrum fuer Schwerionenforschung GmbH on January 10, 2022

SIII) and (*40*). The corresponding transverse magnetization generates a measurable oscillating effective magnetic field on ^{87}Rb magnetometer. As a result, the amplitude of the effective field is

$$|\mathbf{B}_{\mathrm{eff}}^{n}| = \frac{4\pi}{3}\kappa_0 M_0^n P_0^n \gamma_n T_{2n} \; |\mathbf{B}_{\mathrm{ac}}^{\mathrm{exo}}| \tag{5}$$

We define a factor $\eta = \frac{4\pi}{3}\kappa_0 M_0^n P_0^n \gamma_n T_{2n}$ that represents the amplification of the signal from the pseudo-magnetic field. This shows that the signal from the pseudo-magnetic field can be preamplified by the hyperpolarized long-lived ^{129}Xe spins. Specifically, because of large Fermi-contact enhancement factor $\kappa_0 \approx 540$ for ^{129}Xe-^{87}Rb system, η is estimated to be more than 100 (*40*). For ^{3}He-K system, for which the spin-coherence time is much longer (~1000 s) (*20*, *21*, *48*), η can reach 10^4.

We note that the overlapping spin ensemble (e.g., ^{129}Xe-^{87}Rb) is also used in "self-compensating" comagnetometers (*20*, *21*, *49*); however, the present spin-based amplifier is quite different from them (see section SIV). In contrast to comagnetometers that should operate in a specific near-zero bias field, the spin-based amplifier operates in a broad range of bias fields, leading to the difference in the explored frequency range and sensitivity. For example, the self-compensating comagnetometer is insensitive to normal magnetic field and is usually used to search for low-frequency exotic signals, whereas the spin-based amplifier remains sensitive to both magnetic field and pseudo-magnetic field ranging from 1 Hz to 1 kHz, which makes them attractive in searching for new physics predicted by numerous theories beyond the standard model, for example, ultralight axion-like dark matter (*40*).

Experimental setup

Experiments are performed using a setup similar to that of (*40*, *46*), depicted in Fig. 1. We experimentally calibrate the amplification factor η and the corresponding enhanced magnetic field sensitivity of ^{87}Rb magnetometer. For example, the bias field B_z^0 is set as 423 nT, corresponding to ^{129}Xe Larmor frequency $\nu_0 \approx 4.995$ Hz. An oscillating magnetic field of 13.0 pT is applied along *y* to simulate the single-frequency pseudo-magnetic field $B_{\mathrm{ac}}^{\mathrm{exo}} \cos(2\pi\nu t)\hat{y}$. By scanning the oscillation frequency ν near the resonance, the maximum value on resonance is determined as the amplification factor. As shown in Fig. 2A, the signal amplitude is well described by a single-pole band-pass filter model (see inset) (*40*) (see section SIII), yielding the full width at half maximum (FWHM) of 24 mHz. The maximum $\eta \approx 116$ is achieved at $\nu \approx \nu_0 \approx 4.995$ Hz. By taking the response of the spin-based amplifier into account, the magnetic sensitivity of ^{87}Rb magnetometer is enhanced to ≈22 fT/$\sqrt{\mathrm{Hz}}$, whereas the off-resonance sensitivity of ^{87}Rb magnetometer is only about 2 pT/$\sqrt{\mathrm{Hz}}$. Moreover, the enhanced sensitivity is far beyond that of the state-of-the-art magnetometers demonstrated with nuclear spins (*50*, *51*), which are usually limited to a few picotesla sensitivity. Therefore, an atomic magnetometer enhanced with a spin-based amplifier is well suited for resonantly searching for exotic spin- and velocity-dependent interactions.

The pseudo-magnetic field, for example, $\mathbf{B}_j^{\mathrm{exo}} = \mathbf{B}_{4+5}^{\mathrm{exo}}$ is generated by the rotor (see Materials and Methods) in Fig. 1. For a source of unpolarized nucleons, we use a single 112.34-g BGO crystal with a high number density of nucleons (*18*). Driven by a servo motor, the single BGO crystal connected to a 48.76-cm aluminum rod rotates with frequency ν≈4.995 Hz in the *xz* plane. The rotation frequency can be measured through the triggered optoelectronic pulses. The center of the aluminum rod is located 58.32 cm away from the center of the ^{129}Xe vapor cell. The rotating BGO crystal generates a pseudo-magnetic field $\mathbf{B}_{4+5}^{\mathrm{exo}} = B_{4+5}^{y}\hat{y}$ along *y*. As demonstrated in the Supplementary Materials (section SII), the field $B_{4+5}^{y}\hat{y}$ can be decomposed into

$$B_{4+5}^{y} = \sum B_{\mathrm{ac}}^{(N)} \cos(2\pi N\nu t) \tag{6}$$

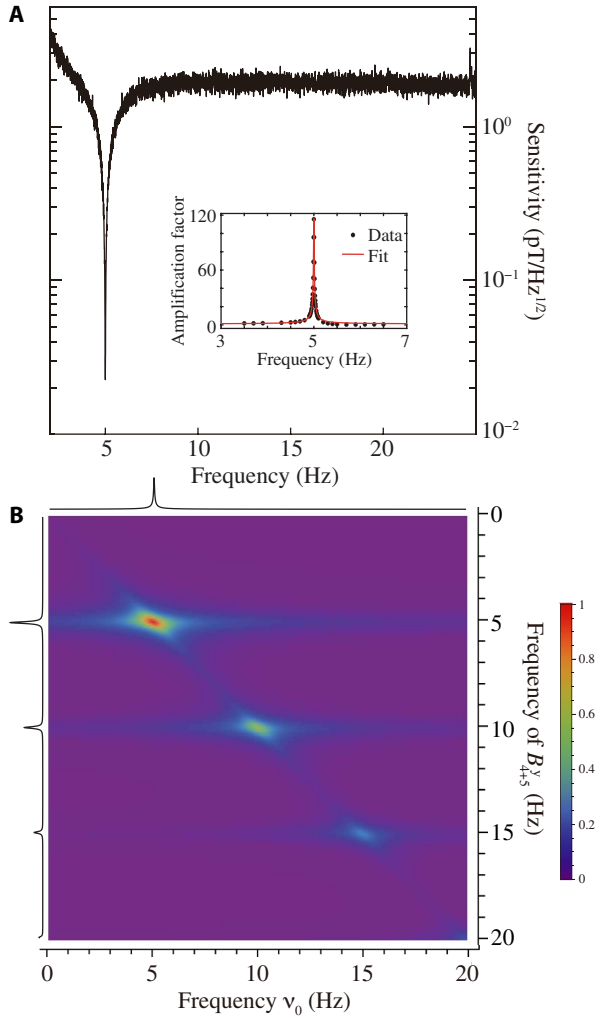

Fig. 2. Demonstration of the spin-based amplifier and basic principle of exotic interaction searches. (**A**) Sensitivity of the spin-amplifier–based magnetometer. The inset exhibits the frequency dependence of the amplification factor. The experimental data (black dots) are obtained by applying a calibration field along *y*. As demonstrated in the Supplementary Materials (section SIII), the red solid line is a theoretical fit of the data with $A/\sqrt{(\nu-\nu_0)^2+(\Lambda/2)^2}$ (*40*), where the FWHM is $\sqrt{3}\,\Lambda \approx 24$ mHz. The enhanced sensitivity of the spin-amplifier–based magnetometer reaches ≈ 22fT/$\sqrt{\mathrm{Hz}}$ at 4.995 Hz. (**B**) Three-dimensional diagram of the enhanced signals from B_{4+5}^{y} with the spin-based amplifier. The *x* axis represents the frequency dependence of the spin-based amplifier [see (A) inset]. The *y* axis represents the decomposition of the pseudo-magnetic field B_{4+5}^{y} generated by the single rotating BGO crystal. By scanning the resonant frequency ν_0 of the spin-based amplifier, there are three peaks of enhanced signals at harmonics of B_{4+5}^{y} with matched frequency $\nu_0 = \nu, 2\nu, 3\nu$. The signal of the pseudo-magnetic field reaches maximum, colored with red, at 4.995 Hz.

Downloaded from https://www.science.org at Helmholtzzentrum fuer Schwerionenforschung GmbH on January 10, 2022

where $N\nu$ is the multiple frequency, and $B_{ac}^{(N)}$ is the corresponding field strength. For example, we consider the case of $\lambda = 1.0$ m and $f_{4+5}^{sim} = 1$ for V_{4+5} generated by the BGO crystal (see Eq. 1). On the basis of our numerical simulation (see Materials and Methods), the ratios of the field strengths at harmonic frequencies are $B_{ac}^{(1)}:B_{ac}^{(2)}:B_{ac}^{(3)} \approx 5.1:2.9:1.4$, as shown in Fig. 2B (y axis). Accordingly, we choose the dominant ($N = 1$) first harmonic $B_{ac}^{(1)}\cos(2\pi\nu t)\hat{y}$ at 4.995 Hz to be measured. To this end, we set the operation frequency of the spin-based amplifier at $\nu_0 \approx 4.995$ Hz. In this situation, because of the relatively narrow bandwidth of the spin-based amplifier, only the signal at 4.995 Hz can be considerably amplified, and the other harmonics are negligible.

Considerable effort is made to reduce undesirable noise, such as air vibration, spurious magnetic noise, electronic cross-talk, etc., before search experiments. For example, the rotating aluminum rod can cause air vibration on the spin-based amplifier, leading to a noise peak at 2ν. To solve this, an enclosure for the spin-based amplifier setup is used to reduce the air vibration effect. Moreover, a single BGO crystal is used, which generates the exotic signal at the frequency of ν and thus avoids the 2ν air vibration effect. While the rotor system is mostly symmetric, the small imbalance due to the single BGO crystal can cause some mechanical vibration. However, we found that this vibration can be neglected in our experiment. We note that the aluminum rod is also a source of unpolarized nucleons, which generates the pseudo-magnetic field consisting of even harmonics at $2N\nu$. The details are presented in the Supplementary Materials (section SII). Nevertheless, the potential pseudo-magnetic field from the aluminum rod can be neglected, because the sensitive frequency of the spin-based amplifier is set at the odd harmonics $\nu \approx 4.995$ Hz. A commercial miniaturized atomic magnetometer is mounted in the vicinity of the vapor cell and used to monitor the spurious magnetic noise (see section SI). To suppress the electronic cross-talk caused by the motor and its control system, all equipment related to the setup of the spin-based amplifier is powered from a different circuit to eliminate all connections between them.

New constraints on V_{4+5} and V_{12+13}

In our experiment, extracting the weak signal with a known carrier frequency from noisy environment is crucial in obtaining the signal from the pseudo-magnetic field. To do this, we use a "lock-in" analysis scheme, similar to the similarity analysis method described in (*19*). The signal is extracted through a reference signal $\cos(2\pi\nu t + \phi)$ obtained from the simulated pseudo-magnetic field. The phase ϕ is the phase delay between the measured magnetic field and the output signal of the spin-based amplifier. The detailed calibration is presented in the Supplementary Materials (section SV). The extracted coupling strength f_{4+5}^{i} of one period T is

$$f_{4+5}^{i} = \frac{1}{\alpha B_{ac}^{(1)}} \frac{\int_0^T \cos(2\pi\nu t + \phi)\, S(t)_i\, dt}{\int_0^T \cos^2(2\pi\nu t + \phi)\, dt} \quad (7)$$

where α is the calibration constant, and $S(t)_i$ is the experimental signal. Here, $B_{ac}^{(1)}$ is the field strength corresponding to $f_{4+5}^{sim} = 1$ for the force range $\lambda = 1.0$ m. To obtain the coupling strength f_{4+5} at a different force range, $B_{ac}^{(1)}$ should be accordingly recalculated (see Materials and Methods).

Histogram of experimentally measured coupling strength f_{4+5}^{i} for 1 hour at 4.995 Hz is shown in Fig. 3. The fit with Gaussian distribution to the histogram gives the mean value and the SE of the coupling strength for 1-hour data $(9.98 \pm 0.83_{stat}) \times 10^{-19}$. The coupling strength collected for 5 hours is $f_{CCW}^{exp} \approx (8.25 \pm 0.35_{stat}) \times 10^{-19}$ for counterclockwise rotation. We note that the mean value of the coupling strength f_{CCW}^{exp} is about 20σ from 0, as shown in Fig. 3. To separate the signal from pseudo-magnetic fields from the spurious signal, we perform the velocity-dependent experiments, where three different frequencies $\nu \approx \{4.114, 4.552, 4.995\}$ Hz are chosen. By extracting the velocity-dependent signal, the velocity-independent spurious signal is greatly suppressed. To further eliminate the velocity-independent spurious signal, we compare the results between clockwise and counterclockwise cycles. After averaging over all rotating circles, the coupling strength is obtained $f_{4+5} \approx (1.08 \pm 2.48_{stat}) \times 10^{-20}$ and $f_{12+13} \approx (1.13 \pm 2.24_{stat}) \times 10^{-35}$. The details are presented in the Supplementary Materials (section SV).

Table 1 summarizes the systematic errors at $\lambda = 1.0$ m in our experiment. The details of calibrating the experimental parameters and obtaining the systematic errors are presented in the Supplementary Materials (section SV). In our experiments, there are two factors leading to the fluctuation of the calibration constant $\delta\alpha$: (i) the intrinsic instability of the spin-based amplifier and (ii) the external instability of the rotor rotation frequency. The intrinsic instability caused by the fluctuation of the laser beam or temperature is $\approx \pm 0.06$ V/nT. Because of the narrow bandwidth of the spin-based amplifier, the instability of the rotation frequency is the dominant fluctuation of the calibration constant, reducing the amplification factor and the corresponding calibration constant. The frequency difference ≈ 0.004 Hz results in $\approx 14\%$ of the reduction of the calibration constant ≈ -0.28 V/nT. The overall systematic uncertainty is derived by combining all the systematic errors in quadrature. Accordingly, we quote the final total coupling strength f_{4+5} as $(1.08 \pm 2.48_{stat} \pm 0.82_{syst}) \times 10^{-20}$. Similarly, $f_{12+13} \approx (1.13 \pm 2.24_{stat} \pm 0.94_{syst}) \times 10^{-35}$ is obtained.

Figure 4 shows the constraints on V_{4+5} and V_{12+13} set by this work. Dark areas represent excluded values with 95% C.L. corresponding to 1.96 times the quadrature of the statistical error and systematic error (see section SV). The previous constraints of f_{4+5} were established with a cold neutron reflectometer (*41*) ($\lambda < 0.04$ m) and a

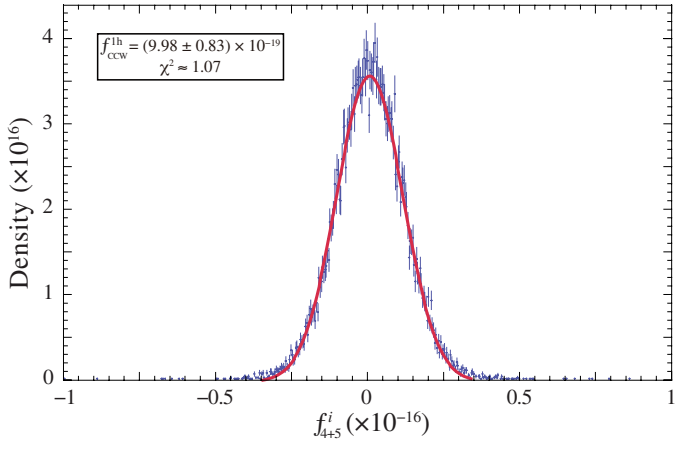

Fig. 3. The histogram of the potential experimental coupling strength f_{4+5}^{i}. Distribution of the experimental coupling strength f_{4+5}^{i} of 1-hour data at $\nu_0 \approx 4.995$ Hz for counterclockwise rotation. The red solid line is a fit to a Gaussian distribution. The $\chi^2 \approx 1.07$ represents a valid fitting.

Downloaded from https://www.science.org at Helmholtzzentrum fuer Schwerionenforschung GmbH on January 10, 2022

Table 1. Summary of systematic errors. The corrections to f_{4+5}^{exp} at λ = 1.0 m are listed.

Parameter	Value	$\Delta f_{4+5}^{exp}(\times 10^{-20})$
Mass of BGO (g)	112.34 ± 0.02	∓0.0002
Position of pivot *x* (mm)	−3.4 ± 0.5	$^{-0.0114}_{+0.0108}$
Position of pivot *y* (mm)	6.0 ± 0.3	±0.0001
Position of pivot *z* (mm)	583.2 ± 1.1	±0.0051
Length of aluminum rod (mm)	487.6 ± 0.7	∓0.0025
Phase delay ϕ (°)	79.1 ± 6.0	$^{-0.6648}_{+0.6533}$
Calib. const. α (V/nT)	$1.91^{+0.06}_{-0.28}$	$^{-0.0274}_{+0.1837}$
Final $f_{4+5}(\times 10^{-20})$	1.08	±2.48 (statistical)
(λ = 1.0 m)		±0.82*

*The origin of coordinates was at the center of the vapor cell.

slow neutron polarimeter (*42*) (λ < 0.01 m). In contrast, our work sets the most stringent constraints on f_{4+5} for the force range from 0.04 to 100 m, as shown in Fig. 4A. For λ=1.0 m, our work improves over previous constraints by about four orders of magnitude. f_{4+5} can be the combination of the scalar neutron coupling with the scalar nucleon coupling. Our work constrains the axion mass 10^{-6} eV$\lesssim m_a \lesssim 7 \times 10^{-6}$ eV, which is within the important axion window (*52*). In Fig. 4B, our work constrains f_{12+13} in the force range from 0.03 to 100 m. Recent works placed constraints with a cold neutron beam (*43*) (λ < 0.06 m) and polarized ^{3}He (*44*) (λ > 4 m). Comparing with them, our work sets the most stringent constraints in the force range from 0.05 to 6 m, at 0.45 m reaching 1.01×10^{-34} (95% C.L.), improving over previous laboratory limits by at least two orders of magnitude.

DISCUSSION

As demonstrated in (*5*, *37*), the spin-dependent interactions between two fermions can be mediated by a massive spin-1 boson *Z*′. The effective Lagrangian of the light boson is

$$\mathcal{L}_{Z'} = Z'_{\mu} \sum_{\psi} \overline{\psi} \gamma^{\mu} (g_v^{\psi} + \gamma_5 g_A^{\psi}) \psi \quad (8)$$

where ψ is the fermion field, and γ^{μ}, γ_5 are Dirac matrices. On the basis of the effective Lagrangian, we can link the coupling strength f_{4+5} and f_{12+13} to the appropriate property of the new bosons, i.e., the product of interaction coupling constants (*37*)

$$f_{4+5}^{Z'} = -\frac{1}{2}\frac{g_A^n g_A^N}{\hbar c} - \frac{3}{2}\frac{g_V^n g_V^N}{\hbar c} \quad (9)$$

$$f_{12+13}^{Z'} = 4\frac{g_A^n g_V^N}{\hbar c} \quad (10)$$

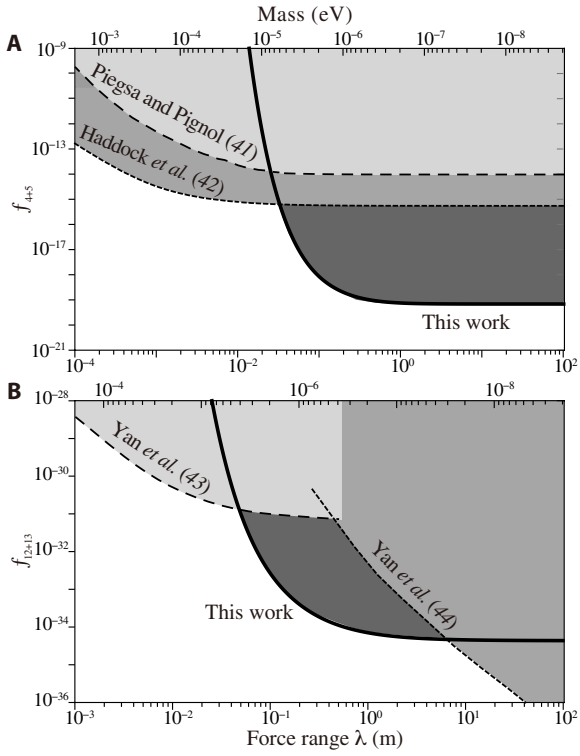

Fig. 4. Constraints (95% C.L.) on f_{4+5} and f_{12+13}. % In (**A**), the dashed lines represent bounds of f_{4+5} from (*41*, *42*). Our work (solid line) sets the most stringent constraints on f_{4+5} for the force range from 0.04 to 100 m. In (**B**), the dashed lines are from (*43*, *44*). The solid line is the constraint of f_{12+13} established by our work, which set the most stringent constraints in the force range from 0.05 to 6 m.

where g_A^n (g_A^N) is the axial-vector interaction coupling constant, and g_V^n (g_V^N) is the vector interaction coupling constant for neutrons (nucleons).

We note that some spin-spin–dependent interactions (e.g., V_{11} and V_3) could also constrain the spin-1 bosons. However, because of the difficulty in preparing polarized nuclear spins with large number and shielding itself from spurious dipole magnetic field, several experiments, so far, addressed the spin-spin–dependent interactions between nucleons, and their search sensitivity was limited (*49*). In contrast, benefiting from the availability of the unpolarized nucleons, the search for V_{12+13} to constrain the spin-1 boson is of experimental interests. We can extract the most stringent limits from direct measurement using the interaction V_{12+13} for spin-1 bosons $g_A^n g_V^N$ for the force range from 0.05 to 0.6 m, not yet competing with combined limits on g_A^n (*49*) and g_V^N (*53*) for these ranges.

Although demonstrated for the spin- and velocity-dependent interactions, the spin-based amplifier is well suited to searching for other exotic interactions, for example, the spin-spin-velocity interactions (V_{6+7}, V_8, V_{14}, V_{15}, and V_{16}). The resonantly oscillating pseudo-magnetic fields can be generated by modulating the relative speed between the source and ^{129}Xe amplifier. Combining our current ^{129}Xe-based amplifier and recently developed $SmCo_5$ spin sources (*19*, *20*), the sensitivity to $|f_{6+7}| < 10^{-20}$, $|f_{14}| < 10^{-31}$, $|f_{15}| < 10^{-4}$, $|f_{16}| < 10^{-4}$ can potentially reach into unexplored parameter space for the force range from 0.01 to 100 m, while for $|f_8| < 10^{-23}$, this is the case for the force range from 0.01 to 1 m. A further improvement of the experimental sensitivity to spin-dependent

Downloaded from https://www.science.org at Helmholtzzentrum fuer Schwerionenforschung GmbH on January 10, 2022

interactions can be anticipated by using ^{3}He noble gas as the spin-based amplifier, which has much longer spin-coherence time and larger gyromagnetic ratio than those of ^{129}Xe (*49*). Using ^{3}He-K systems, the projected magnetic sensitivity to those spin-dependent interactions can be improved by four orders of magnitude (*40*). The details are presented in the Supplementary Materials (see section SVI).

In this work, we have reported new constraints, based on a spin-based amplifier, on exotic spin- and velocity-dependent interactions. Using our spin-based amplifier technique, we anticipate that our work will stimulate interesting new research for new nuclear physics predicted by numerous theories beyond the standard model, for example, the searches for axion-like particles (*40*) and dark photons (*6*).

MATERIALS AND METHODS

Experimental setup

The exotic spin- and velocity-dependent interactions V_{4+5} and V_{12+13} are generated by a single cube-shaped BGO crystal with 25.0 × 25.0 × 25.0 mm^3 total volume. The 112.34-g BGO crystal is mounted in a box at one end of a symmetric aluminum rod (see Fig. 1). The center of the 48.76-cm aluminum rod is located 58.32 cm away from the center of the ^{129}Xe vapor cell. The center of the aluminum rod is connected to a servo motor fixed on a stable aluminum platform, through a cylindrical titanium rod. Driven by the motor, the BGO cystal and the aluminum rod rotate with a frequency $\nu \approx 4.995$ Hz in the *xz* plane. To precisely determine the rotation frequency ν, a bronze needle is fixed on the titanium rod to trigger pulses when passing through the optoelectronic switch. Specific design details and the schematic figure of the rotor can be found in the Supplementary Materials (section SI).

Simulation of the pseudo-magnetic fields

To obtain the reference signal for lock-in analysis scheme, we simulate the pseudo-magnetic fields $\mathbf{B}^{\mathrm{exo}}_{4+5}$ and $\mathbf{B}^{\mathrm{exo}}_{12+13}$ before data analysis. The pseudo-magnetic field $\mathbf{B}^{\mathrm{exo}}_{4+5}$ can be obtained by integrating over the whole volume of the BGO crystal

$$\mathbf{B}^{\mathrm{exo}}_{4+5} = f_{4+5}\frac{\hbar^2}{8\pi mc\,|\,\boldsymbol{\mu}_{\mathrm{Xe}}\,|}\iiint\rho(\boldsymbol{r})\,(\boldsymbol{v}\times\hat{r})\left(\frac{1}{\lambda r}+\frac{1}{r^2}\right)e^{-r/\lambda}d\boldsymbol{r} \quad (11)$$

where $\rho(\boldsymbol{r})$ is the BGO crystal's nucleon density at location $\boldsymbol{r}$, and m is the mass of a neutron. The pseudo-magnetic field $\mathbf{B}^{\mathrm{exo}}_{4+5} = B^{y}_{4+5}\hat{y}$ is not a pure trigonometric function containing the harmonics of ν (i.e., ν, 2ν, and 3ν). In our experiment, because of the relatively narrow bandwidth ≈24 mHz of the spin-based amplifier, only the first harmonic [i.e., $B^{(1)}_{\mathrm{ac}}\cos(2\pi\nu t)\,\hat{y}$] can be resonantly amplified, and other harmonics can be neglected. Hence, we filter the simulated signal and obtain the first harmonic $B^{(1)}_{\mathrm{ac}}\cos(2\pi\nu t+\phi)\,\hat{y}$ as the reference signal, which is demonstrated in the Supplementary Materials (section SII).

The pseudo-magnetic field $\mathbf{B}^{\mathrm{exo}}_{12+13}$ can be derived by the same method demonstrated above

$$\mathbf{B}^{\mathrm{exo}}_{12+13} = -f_{12+13}\frac{\hbar}{8\pi\,|\,\boldsymbol{\mu}_{\mathrm{Xe}}\,|}\iiint\rho(\hat{r})\,(\boldsymbol{v})\left(\frac{1}{r}\right)e^{-r/\lambda}d\boldsymbol{r} \quad (12)$$

In contrast to $\mathbf{B}^{\mathrm{exo}}_{4+5}$, the pseudo-magnetic field $\mathbf{B}^{\mathrm{exo}}_{12+13} = B^{x}_{12+13}\hat{x} + B^{z}_{12+13}\hat{z}$ contains two components along *x* and *z*. We note that the spin-based amplifier is insensitive to the oscillating field along *z*, because the oscillating field along *z* cannot induce ^{129}Xe transverse magnetization. Therefore, only the *x* component of the pseudo-magnetic field $B^{x}_{12+13}\hat{x}$ should be considered. Considering the bandwidth of the spin-based amplifier, we filter the simulated signal and obtain the first harmonic $B^{(1)}_{\mathrm{ac}}\cos(2\pi\nu t+\phi)\,\hat{x}$ as reference signal, which is demonstrated in the Supplementary Materials (section SII).

Data analysis

In our experiment, the lock-in analysis scheme is applied to extract the coupling strengths f_{4+5} and f_{12+13}. The experimental signal $S(t)$ is filtered around the resonance frequency and separated into segments of one period $S(t)_i$. The reference signal of one period is obtained by applying the same filter to the simulated pseudo-magnetic field. After performing the lock-in analysis scheme and extracting the coupling strength f^{i}_{4+5}, the histogram of all the experimental coupling strengths is obtained. The fit with Gaussian distribution to the histogram gives the mean value and the SE of the coupling strength for 1-hour data. By averaging the five coupling strengths and calculating the uncertainty propagation, we obtain the coupling strength for 5-hour data.

It is important to separate the exotic signal generated by spin-dependent interactions from the spurious signal. First, to eliminate the velocity-independent spurious signal, we perform velocity-dependent experiments by changing the rotation frequency ν of the BGO rotor. According to the mathematical structure of V_{4+5}, V_{12+13}, the signal from the pseudo-magnetic fields should be proportional to the rotation frequency. Therefore, after obtaining the coupling strength $f^{\mathrm{exp}}_{\mathrm{CCW}}$ at different frequencies $\nu \approx \{4.114, 4.552, 4.995\}$ Hz, the coupling strength f_{CCW} for counterclockwise cycles is extracted by using a theoretical fit. After the fit, we extract the velocity-dependent signal including the signal from spin-dependent interactions and the velocity-dependent spurious signal. To further eliminate the spurious signal, we compare the results between clockwise and counterclockwise cycles. On the basis of the lock-in analysis scheme, the coupling strength is independent of rotation direction, whereas the velocity-dependent spurious signal is reversed for counterclockwise and clockwise cycles. If the velocity-dependent spurious signal dominates, we should observe that f_{CCW} and f_{CW} have reversed sign. The coupling strength of clockwise and counterclockwise cycles shows a reversed sign as expected, for example, $f_{\mathrm{CW}} \approx (2.41 \pm 0.34_{\mathrm{stat}}) \times 10^{-19}$ and $f_{\mathrm{CCW}} \approx (-2.19 \pm 0.35_{\mathrm{stat}}) \times 10^{-19}$ for the force range $\lambda = 1.0$ m. After averaging over all rotating circles, the coupling strength is obtained $f_{4+5} \approx (1.08 \pm 2.48_{\mathrm{stat}}) \times 10^{-20}$. In the same way, $f_{12+13} \approx (1.13 \pm 2.24_{\mathrm{stat}}) \times 10^{-35}$ can be obtained. The detailed process is presented in the Supplementary Materials (section SV).

SUPPLEMENTARY MATERIALS

Supplementary material for this article is available at https://science.org/doi/10.1126/sciadv.abi9535

REFERENCES AND NOTES

1. N. F. Ramsey, The tensor force between two protons at long range. *Phys. Ther.* **96**, 285–289 (1979).
2. F. Wilczek, Problem of strong *P* and *T* invariance in the presence of instantons. *Phys. Rev. Lett.* **40**, 279–282 (1978).
3. R. D. Peccei, H. R. Quinn, CP conservation in the presence of pseudoparticles. *Phys. Rev. Lett.* **38**, 1440–1443 (1977).
4. S. Weinberg, A new light boson? *Phys. Rev. Lett.* **40**, 223–226 (1978).

Downloaded from https://www.science.org at Helmholtzzentrum fuer Schwerionenforschung GmbH on January 10, 2022

5. P. Fadeev, Y. V. Stadnik, F. Ficek, M. G. Kozlov, V. V. Flambaum, D. Budker, Revisiting spin-dependent forces mediated by new bosons: Potentials in the coordinate-space representation for macroscopic-and atomic-scale experiments. *Phys. Rev. A* **99**, 022113 (2019).
6. H. An, M. Pospelov, J. Pradler, A. Ritz, Direct detection constraints on dark photon dark matter. *Phys. Lett. B* **747**, 331–338 (2015).
7. B. A. Dobrescu, Massless gauge bosons other than the photon. *Phys. Rev. Lett.* **94**, 151802 (2005).
8. R. Ammar; CLEO Collaboration, Search for the familon via $B^{\pm} \rightarrow \pi^{\pm} X^0$, $B^{\pm} \rightarrow K^{\pm} X^0$, and $B^0 \rightarrow K_s^0 X^0$ decays. *Phys. Rev. Lett.* **87**, 271801 (2001).
9. D. S. Dearborn, D. N. Schramm, G. Steigman, Astrophysical constraints on the couplings of axions, majorons, and familons. *Phys. Rev. Lett.* **56**, 26–29 (1986).
10. D. DeMille, J. M. Doyle, A. O. Sushkov, Probing the frontiers of particle physics with tabletop-scale experiments. *Science* **357**, 990–994 (2017).
11. M. S. Safronova, D. Budker, D. DeMille, D. F. J. Kimball, A. Derevianko, C. W. Clark, Search for new physics with atoms and molecules. *Rev. Mod. Phys.* **90**, 025008 (2018).
12. W. A. Terrano, E. G. Adelberger, J. G. Lee, B. R. Heckel, Short-range, spin-dependent interactions of electrons: A probe for exotic pseudo-goldstone bosons. *Phys. Rev. Lett.* **115**, 201801 (2015).
13. J. Ding, J. Wang, X. Zhou, Y. Liu, K. Sun, A. O. Adeyeye, H. Fu, X. Ren, S. Li, P. Luo, Z. Lan, S. Yang, J. Luo, Constraints on the velocity and spin dependent exotic interaction at the micrometer range. *Phys. Rev. Lett.* **124**, 161801 (2020).
14. D. J. Wineland, J. J. Bollinger, D. J. Heinzen, W. M. Itano, M. G. Raizen, Search for anomalous spin-dependent forces using stored-ion spectroscopy. *Phys. Rev. Lett.* **67**, 1735–1738 (1991).
15. S. Kotler, R. Ozeri, D. F. J. Kimball, Constraints on exotic dipole-dipole couplings between electrons at the micrometer scale. *Phys. Rev. Lett.* **115**, 081801 (2015).
16. L. Hunter, J. Gordon, S. Peck, D. Ang, J.-F. Lin, Using the earth as a polarized electron source to search for long-range spin-spin interactions. *Science* **339**, 928–932 (2013).
17. L. R. Hunter, D. G. Ang, Using geoelectrons to search for velocity-dependent spin-spin interactions. *Phys. Rev. Lett.* **112**, 091803 (2014).
18. Y. J. Kim, P.-H. Chu, I. Savukov, S. Newman, Experimental limit on an exotic parity-odd spin-and velocity-dependent interaction using an optically polarized vapor. *Nat. Commun.* **10**, 2245 (2019).
19. W. Ji, Y. Chen, C. Fu, M. Ding, J. Fang, Z. Xiao, K. Wei, H. Yan, New experimental limits on exotic spin-spin-velocity-dependent interactions by using $SmCo_5$ spin sources. *Phys. Rev. Lett.* **121**, 261803 (2018).
20. A. Almasi, J. Lee, H. Winarto, M. Smiciklas, M. V. Romalis, New limits on anomalous spin-spin interactions. *Phys. Rev. Lett.* **125**, 201802 (2020).
21. J. Lee, A. Almasi, M. Romalis, Improved limits on spin-mass interactions. *Phys. Rev. Lett.* **120**, 161801 (2018).
22. X. Rong, M. Wang, J. Geng, X. Qin, M. Guo, M. Jiao, Y. Xie, P. Wang, P. Huang, F. Shi, Y. F. Cai, C. Zou, J. Du, Searching for an exotic spin-dependent interaction with a single electron-spin quantum sensor. *Nat. Commun.* **9**, 739 (2018).
23. X. Rong, M. Jiao, J. Geng, B. Zhang, T. Xie, F. Shi, C. K. Duan, Y. F. Cai, J. Du, Constraints on a spin-dependent exotic interaction between electrons with single electron spin quantum sensors. *Phys. Rev. Lett.* **121**, 080402 (2018).
24. M. Jiao, M. Guo, X. Rong, Y.-F. Cai, J. Du, Experimental constraint on an exotic parity-odd spin-and velocity-dependent interaction with a single electron spin quantum sensor. *Phys. Rev. Lett.* **127**, 010501 (2020).
25. M. Bulatowicz, R. Griffith, M. Larxen, J. Mirijanian, C. B. Fu, E. Smith, W. M. Snow, H. Yan, T. G. Walker, Laboratory search for a long-range *T*-odd, *P*-odd interaction from axionlike particles using dual-species nuclear magnetic resonance with polarized ^{129}Xe and ^{131}Xe gas. *Phys. Rev. Lett.* **111**, 102001 (2013).
26. K. Tullney, F. Allmendinger, M. Burghoff, W. Heil, S. Karpuk, W. Kilian, S. Knappe-Grüneberg, W. Müller, U. Schmidt, A. Schnabel, F. Seifert, Y. Sobolev, L. Trahms, Constraints on spin-dependent short-range interaction between nucleons. *Phys. Rev. Lett.* **111**, 100801 (2013).
27. F. Ficek, D. F. J. Kimball, M. G. Kozlov, N. Leefer, S. Pustelny, D. Budker, Constraints on exotic spin-dependent interactions between electrons from helium fine-structure spectroscopy. *Phys. Rev. A* **95**, 032505 (2017).
28. F. Ficek, P. Fadeev, V. V. Flambaum, D. F. Jackson Kimball, M. G. Kozlov, Y. V. Stadnik, D. Budker, Constraints on exotic spin-dependent interactions between matter and antimatter from antiprotonic helium spectroscopy. *Phys. Rev. Lett.* **120**, 183002 (2018).
29. W.-T. Ni, S.-S. Pan, H.-C. Yeh, L.-S. Hou, J. Wan, Search for an axionlike spin coupling using a paramagnetic salt with a dc SQUID. *Phys. Rev. Lett.* **82**, 2439 (1999).
30. D. J. Kimball, A. Boyd, D. Budker, Constraints on anomalous spin-spin interactions from spin-exchange collisions. *Phys. Rev. A* **82**, 062714 (2010).
31. Y. V. Stadnik, V. A. Dzuba, V. V. Flambaum, Improved limits on axionlike-particle-mediated *P, T*-violating interactions between electrons and nucleons from electric dipole moments of atoms and molecules. *Phys. Rev. Lett.* **120**, 013202 (2018).
32. V. A. Dzuba, V. V. Flambaum, I. B. Samsonov, Y. V. Stadnik, New constraints on axion-mediated *P,T*-violating interaction from electric dipole moments of diamagnetic atoms. *Phys. Rev. D* **98**, 035048 (2018).
33. A. Arvanitaki, A. A. Geraci, Resonantly detecting axion-mediated forces with nuclear magnetic resonance. *Phys. Rev. Lett.* **113**, 161801 (2014).
34. P.-H. Chu, Y. J. Kim, I. M. Savukov, Search for exotic spin-dependent interactions using polarized helium. arXiv:2002.02495 [nucl-ex] (6 February 2020).
35. N. Aggarwal, A. Schnabel, J. Voigt, A. Brown, J. C. Long, L. Trahms, A. Fang, A. Geraci, A. Kapitulnik, D. Kim, Y. Kim, I. Lee, Y. H. Lee, C. Y. Liu, C. Lohmeyer, A. Reid, Y. Semertzidis, Y. Shin, J. Shortino, E. Smith, W. M. Snow, E. Weisman, Characterization of magnetic field noise in the ARIADNE source mass rotor. arXiv:2011.12617 [physics.ins-det] (25 November 2020).
36. J. Moody, F. Wilczek, New macroscopic forces? *Phys. Rev. D* **30**, 130–138 (1984).
37. B. A. Dobrescu, I. Mocioiu, Spin-dependent macroscopic forces from new particle exchange. *J. High Energy Phys.* **2006**, 005 (2006).
38. T. M. Leslie, E. Weisman, R. Khatiwada, J. C. Long, Prospects for electron spin-dependent short-range force experiments with rare earth iron garnet test masses. *Phys. Rev. D* **89**, 114022 (2014).
39. G. P. de Brito, P. C. Malta, L. P. R. Ospedal, Spin- and velocity-dependent nonrelativistic potentials in modified electrodynamics. *Phys. Rev. D* **95**, 016006 (2017).
40. M. Jiang, H. Su, A. Garcon, X. Peng, D. Budker, Search for axion-like dark matter with spin-based amplifiers. arXiv:2102.01448 [hep-ph] (2 February 2021).
41. F. M. Piegsa, G. Pignol, Limits on the axial coupling constant of new light bosons. *Phys. Rev. Lett.* **108**, 181801 (2012).
42. C. Haddock, J. Amadio, E. Anderson, L. Barrón-Palos, B. Crawford, C. Crawford, D. Esposito, W. Fox, I. Francis, J. Fry, H. Gardiner, A. Holley, K. Korsak, J. Lieffers, S. Magers, M. Maldonado-Velázquez, D. Mayorov, J. S. Nico, T. Okudaira, C. Paudel, S. Santra, M. Sarsour, H. M. Shimizu, W. M. Snow, A. Sprow, K. Steffen, H. E. Swanson, F. Tovesson, J. Vanderwerp, P. A. Yergeau, A search for possible long range spin dependent interactions of the neutron from exotic vector boson exchange. *Phys. Lett. B* **783**, 227–233 (2018).
43. H. Yan, W. Snow, New limit on possible long-range parity-odd interactions of the neutron from neutron-spin rotation in liquid ^{4}He. *Phys. Rev. Lett.* **110**, 082003 (2013).
44. H. Yan, G. A. Sun, S. M. Peng, Y. Zhang, C. Fu, H. Guo, B. Q. Liu, Searching for new spin-and velocity-dependent interactions by spin relaxation of polarized ^{3}He gas. *Phys. Rev. Lett.* **115**, 182001 (2015).
45. D. J. Kimball, Nuclear spin content and constraints on exotic spin-dependent couplings. *New J. Phys.* **17**, 073008 (2015).
46. M. Jiang, H. Su, Z. Wu, X. Peng, D. Budker, Floquet maser. *Sci. Adv.* **7**, eabe0719 (2021).
47. T. G. Walker, W. Happer, Spin-exchange optical pumping of noble-gas nuclei. *Rev. Mod. Phys.* **69**, 629–642 (1997).
48. T. W. Kornack, R. K. Ghosh, M. V. Romalis, Nuclear spin gyroscope based on an atomic comagnetometer. *Phys. Rev. Lett.* **95**, 230801 (2005).
49. G. Vasilakis, J. M. Brown, T. Kornack, M. V. Romalis, Limits on new long range nuclear spin-dependent forces set with a K-^{3}He comagnetometer. *Phys. Rev. Lett.* **103**, 261801 (2009).
50. S. Gross, C. Barmet, B. E. Dietrich, D. O. Brunner, T. Schmid, K. P. Pruessmann, Dynamic nuclear magnetic resonance field sensing with part-per-trillion resolution. *Nat. Commun.* **7**, 13702 (2016).
51. T. Wu, J. W. Blanchard, D. F. J. Kimball, M. Jiang, D. Budker, Nuclear-spin comagnetometer based on a liquid of identical molecules. *Phys. Rev. Lett.* **121**, 023202 (2018).
52. M. S. Turner, Windows on the axion. *Phys. Rep.* **197**, 67–97 (1990).
53. J. K. Hoskins, R. D. Newman, R. Spero, J. Schultz, Experimental tests of the gravitational inverse-square law for mass separations from 2 to 105 cm. *Phys. Rev. D* **32**, 3084–3095 (1985).
54. D. Budker, D. F. J. Kimball, *Optical Magnetometry* (Cambridge Univ. Press, 2013), chap. 12.
55. M. Jiang, W. Xu, Q. Li, Z. Wu, D. Suter, X. Peng, Interference in atomic magnetometry. *Adv. Quantum Technol.* **3**, 2000078 (2020).
56. Z. K. Wu, M. Kitano, W. Happer, M. Hou, J. M. Daniels, Optical determination of alkali metal vapor number density using faraday rotation. *Appl. Optics* **25**, 4483–4492 (1986).
57. W. Opechowski, Magneto-optical effects and paramagnetic resonance. *Rev. Mod. Phys.* **25**, 264–268 (1953).

Acknowledgments: We thank Y. K. Semertzidis, X. Rong, Y. V. Stadnik, D. Kim, Y. Kim, Y. Chen, and Y. C. Shin for valuable discussions. **Funding:** The work of H.S., Y.W., M.J., and X.P. was supported by the National Key Research and Development Program of China (grant no. 2018YFA0306600), National Natural Science Foundation of China (grants nos. 11661161018, 11927811, and 12004371), Anhui Initiative in Quantum Information Technologies (grant no. AHY050000), and USTC Research Funds of the Double First-Class Initiative (grant no. YD3540002002). The work of D.B. and P.F. was supported by the Cluster of Excellence PRISMA+ funded by the German Research Foundation (DFG) within the German Excellence

Downloaded from https://www.science.org at Helmholtzzentrum fuer Schwerionenforschung GmbH on January 10, 2022

Strategy (Project ID 39083149), by the European Research Council (ERC) under the European Union Horizon 2020 research and innovation program (project Dark-OST, grant agreement no. 695405), and by the DFG Reinhart Koselleck project. **Author contributions:** M.J., X.P., and D.B. proposed the experimental concept, devised the experimental protocols, and wrote the manuscript. H.S. and Y.W. designed and performed experiments, analyzed the data, and wrote the manuscript. W.J. and P.F. analyzed the data, added theoretical discussion, and edited the manuscript. D.H. assisted in designing the rotating setup. All authors contributed with discussions and checking the manuscript. **Competing interests:** The authors declare that they have no competing interests. **Data and materials availability:** All data needed to evaluate the conclusions in the paper are present in the paper and/or the Supplementary Materials.

Submitted 11 April 2021
Accepted 28 September 2021
Published 17 November 2021
10.1126/sciadv.abi9535

Downloaded from https://www.science.org at Helmholtzzentrum fuer Schwerionenforschung GmbH on January 10, 2022

ScienceAdvances

Search for exotic spin-dependent interactions with a spin-based amplifier

Haowen SuYuanhong WangMin JiangWei JiPavel FadeevDongdong HuXinhua PengDmitry Budker

Sci. Adv., 7 (47), eabi9535. • DOI: 10.1126/sciadv.abi9535

View the article online
https://www.science.org/doi/10.1126/sciadv.abi9535
Permissions
https://www.science.org/help/reprints-and-permissions

Downloaded from https://www.science.org at Helmholtzzentrum fuer Schwerionenforschung GmbH on January 10, 2022

Use of think article is subject to the Terms of service

Science Advances (ISSN) is published by the American Association for the Advancement of Science. 1200 New York Avenue NW, Washington, DC 20005. The title *Science Advances* is a registered trademark of AAAS.
Copyright © 2021 The Authors, some rights reserved; exclusive licensee American Association for the Advancement of Science. No claim to original U.S. Government Works. Distributed under a Creative Commons Attribution NonCommercial License 4.0 (CC BY-NC).